Burned area detection based on Landsat time series in savannas of southern Burkina Faso

Jinxiu Liu[1,*], Janne Heiskanen[1], Eduardo Eiji Maeda[2], Petri K.E. Pellikka[1]

[1]Department of Geosciences and Geography, P.O. Box 68, FI-00014, University of Helsinki, Finland

[2]Department of Environmental Sciences, Fisheries and Environmental Management Group, P.O. Box 68, FI-00014, University of Helsinki, Finland

*Corresponding author. E-mail: jinxiu.liu@helsinki.fi

Abstract

West African savannas are subject to regular fires, which have impacts on vegetation structure, biodiversity and carbon balance. An efficient and accurate mapping of burned area associated with seasonal fires can greatly benefit decision making in land management. Since coarse resolution burned area products cannot meet the accuracy needed for fire management and climate modelling at local scales, the medium resolution Landsat data is a promising alternative for local scale studies. In this study, we developed an algorithm for continuous monitoring of annual burned areas using Landsat time series. The algorithm is based on burned pixel detection using harmonic model fitting with Landsat time series and breakpoint identification in the time series data. This approach was tested in a savanna area in southern Burkina Faso using 281 images acquired between October 2000 and April 2016. An overall accuracy of 79.2% was obtained with balanced omission and commission errors. This represents a significant improvement in comparison with MODIS burned area product (67.6%), which had more omission errors than commission errors, indicating underestimation of the total burned area. By observing the spatial distribution of burned areas, we found that the Landsat based method misclassified cropland and cloud shadows as burned areas due to the similar spectral response, and MODIS burned area product omitted small and fragmented burned areas. The proposed algorithm is flexible and robust against decreased data availability caused by clouds and Landsat 7 missing lines, therefore having a high potential for being applied in other landscapes in future studies.

Keywords: burned area, Landsat time series, harmonic model, breakpoint identification, MODIS

1 Introduction

Fire is recognized as one of the most important ecosystem disturbances, as it contributes to determining vegetation structure, biodiversity and carbon balance (Nielsen and Rasmussen, 1997; Mouillot et al., 2014, Giglio et al., 2010). In the African savanna, fires burn extensive areas annually, and account for a large proportion of the global extent of burned areas (Dwyer et al., 2000). In addition, fires in Africa are driven by factors such as rainfall, tree cover and population density (Archibald et al., 2009). Therefore, accurate mapping of burned areas in savannas is crucial for social and environmental applications (Boschetti et al., 2015).

Remote sensing plays a key role in monitoring burned area at regional and global scales. Due to the high temporal resolution and large spatial coverage, the current burned area products rely on coarse spatial resolution satellite data. A number of global burned area products have been made available, for example, MODIS (Moderate Resolution Imaging Spectroradiometer) burned area product (MCD45A1) based on Terra and Aqua MODIS data at 500 m spatial resolution (Roy et al., 2008), L3JRC burned area product based on SPOT VEGETATION data at 1 km spatial resolution (Tansey et al., 2008), and 1 km Globcarbon burned area product derived from SPOT VEGETATION, ERS2-ATSR2 and ENVISAT AATSR data (Plummer et al., 2006). However, the global burned area products with a coarse spatial resolution fail to detect small and patchy fires, and are not detailed and accurate enough for climate modelling and fire management at regional and local scales (Smith et al., 2007; Roy et al., 2009; Bastarrika et al., 2011).

Medium spatial resolution imagery provides the much needed improvement in spatial resolution of burned area mapping although global product has not been produced yet. For example, the Landsat satellite image archive stores more than four decades of multispectral observations across the planet, having a high potential for studying fire dynamics. Current methods of burned area detection include manual interpretation and digitalization (Silva et al. 2005), decision tree classification (Kontoes et al., 2009), principal component analysis (Koutsias et al. 2009), artificial neural networks (Maeda et al., 2009), logistic regression (Siljander 2009), thresholding based on post-fire image (Koutsias et al., 2013) or pre-fire and post-fire images (Kontoes et al., 2009; Maeda et al., 2011; Bastarrika et al., 2014), and region growing segmentation (Hardtke et al., 2015). However, most studies have employed spectral differences between pre-fire and post-fire images for burned area mapping and fire severity study. The spectral indices, such as normalized burned ratio (NBR), burned area index (BAI), mid infrared burn index (MIRBI) and global environmental monitoring index (GEMI) have commonly been used to make such comparisons (Chuvieco et al., 2002; Bastarrika et al., 2011, Musyimi et al., 2017; Schepers et al., 2014). Moreover, it was indicated from previous studies that

the widely used NBR is less sensitive to burn scars in savanna environments (Goodwin and Collett 2014; Disney et al., 2011), and BAI has been applied effectively for burned area discrimination including savanna area in Africa in previous studies (Chuvieco et al., 2002; Bastarrika et al., 2011; Dempewolf et al., 2007).

However, the approach based on image comparison is hampered by several issues. First, it can be difficult to obtain suitable pre-fire and post-fire images over large areas due to cloud contamination. A manual image selection process is often required to minimize the phenology effect between the image pairs. Second, burned areas demonstrate a spatial and spectral diversity due to the burned vegetation type, fire severity, and the time difference between the image acquisition date and fire date (Stroppiana et al., 2012). During fire seasons, old burn scars are less obvious in comparison to new ones, given the rapid recovery of vegetation. Cloud shadows, water bodies and agricultural areas also exhibit a similar spectral response to burned areas and result in commission errors (Boschetti et al., 2015). Although the image comparison method can achieve good results for a particular region, it can be difficult to apply over large areas. Therefore, more automated approaches for burned area mapping are needed without the limitations of two image comparisons.

With open access to the image archive, Landsat time series have become an important source of medium resolution data for land cover characterization and monitoring. Several time series approaches have been used to identify forest disturbance, clouds and cloud shadows. Zhu and Woodcock (2014b) proposed an algorithm based on harmonic models to automatically remove pixels contaminated by cloud, cloud shadow and snow. Goodwin and Collett (2014) developed an automated method for burned area mapping in Queensland, Australia. The method included detection of outliers caused by burned vegetation, region growing segmentation to map the changed areas, and the classification tree to separate burn scars from other changes. Liu et al. (2016) used seasonal features from an annual Landsat time series for land cover characterization. The harmonic model was used to detect outliers caused by burn scars. However, the use of Landsat time series to monitor long-term burn area dynamics has not been comprehensively studied. Furthermore, burned area detection with medium resolution in a continuous and automatic way has been rarely applied to Landsat time series in savanna area where fires occur frequently.

African savannas are experiencing land cover changes, which must be addressed if burned area detection is applied to long time series. Liu et al. (2016) showed that parameters of the harmonic model vary between land cover types in the savannas of Burkina Faso, particularly between woodlands and cropland. Therefore, the conversion of woodlands to cropland, which is the prevailing land use and land cover change type in the region (Knauer et al., 2017), affects the seasonality of BAI,

and for reliable burn scar detection, it is necessary to define periods with stable land cover before model fitting. DeVries et al. (2015) applied an automatic algorithm to track tropical deforestation and degradation in southern Ethiopia based on Landsat normalized difference vegetation index (NDVI) time series data. The algorithm is based on the BFAST method (Verbesselt et al., 2012) and can potentially provide time series breakpoint identification required for burned area detection, although this remains to be tested.

In this study, our objective was to develop and evaluate an algorithm based on harmonic model and time series breakpoint identification to detect annual burned area using Landsat time series. The method was tested in southern Burkina Faso using all available Landsat imagery between 2000 and 2016. Furthermore, the potential of Landsat time series in burned area mapping was compared with MODIS burned area product.

2 Material and method

2.1 Study area

The study area is located in southern Burkina Faso in the Ziro and Sissili provinces (Fig. 1) and belongs to the West Sudanian savanna ecoregion (Olson et al., 2001). The mean annual precipitation was 827 mm and the mean annual temperature was 27.5 °C in 1950–2000 (Hijmans et al., 2005). Most of the precipitation falls between May and September, the wettest month being August. The driest months are December, January and February. The topography is relatively flat with a mean elevation of 350 m above sea level. The land cover include tropical dry forests and woodlands which are surrounded by agroforestry parklands and agriculture (Liu et al., 2016). The ground layer is dominated by perennial grasses. Forests are partly under community forest management and protection, aiming at providing sustainable fuelwood (Coulibaly-Lingani et al., 2011). The farming system is a mixture of traditional subsistence farming of, for example, sorghum, millet and maize, and cultivation of cash crops, such as cotton, sesame and peanuts. Due to the immigration of farmers, southern Burkina Faso has experienced a rapid population growth with increasing conversion of forests and woodland into cropland during the last decade (Ouedraogo et al., 2009; Gessner et al., 2015). A high level of deforestation and fragmentation exists in southern Burkina Faso, and management plans to ensure the sustainable use of forest resources are needed (Ouedraogo et al., 2011).

Fires due to anthropogenic and natural causes take place regularly in this region (Sawadogo et al., 2002). Most of the fires occur during the dry season in November, December, January, and February, even in early October, and very late March and April (Gessner et al., 2015). The length of fire season

differs from year to year, and the variations exist in the starting and ending months of the fire season. The early fires are fragment with low intensity because the herbaceous layer still holds moisture from the wet season (Sawadogo et al., 2005). Late fires are fierce and devastating which can cause burn scars in a large and contiguous pattern (Sawadogo et al., 2002). Fires do not cause permanent land cover change, and burned vegetation typically recovers quickly (Silva et al., 2005). It is widely understood that ashes can release minerals which promote herbaceous production, and the fire regime is also regarded as having significant implications in maintaining species composition and biodiversity of the savannas (Sawadogo et al., 2005; Laris et al., 2006).

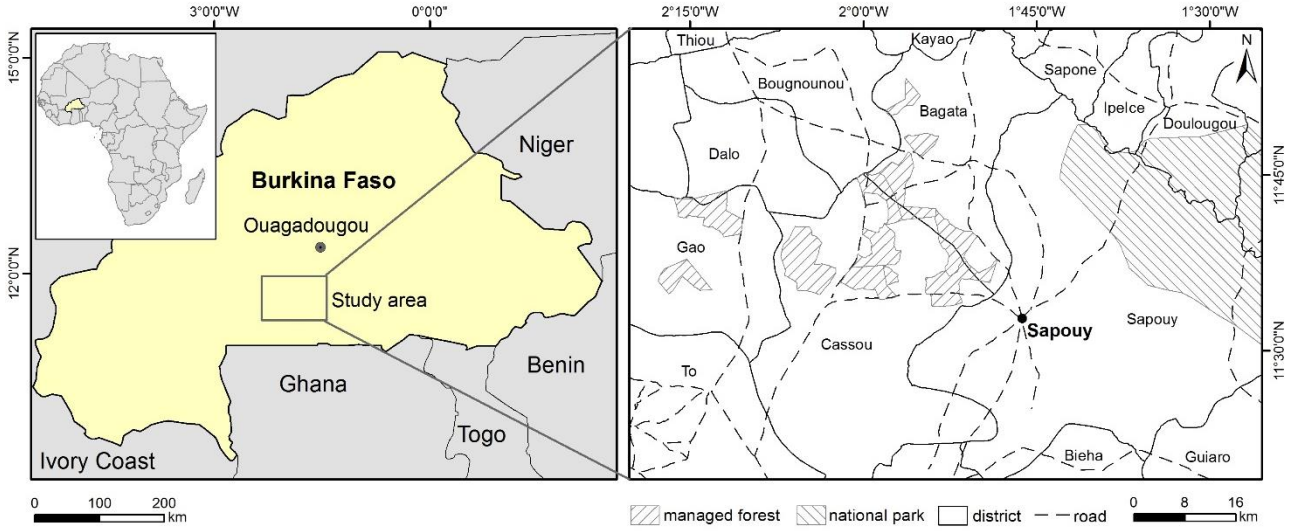

Fig. 1. The location of study area.

2.2 Data

We downloaded all available Landsat Surface Reflectance data with WRS-2 coordinates Path 195 Row 52 between October 2000 and April 2016 from the Earth Resources Observations and Science (EROS) Center archive. A total of 281 images including 40 Landsat 5 Thematic Mapper (TM) images, 185 Landsat 7 Enhanced Thematic Mapper Plus (ETM+) images, and 56 Landsat 8 Operational Land Imager (OLI) images were used. The products have been atmospherically corrected and clouds and shadows have been detected with Fmask algorithm (Zhu and Woodcock, 2012). We selected blue, green, red, near-infrared (NIR) and two shortwave infrared (SWIR1, SWIR2) bands for further analysis.

2.3 Burned area detection algorithm

An overview of the algorithm for detecting the annual burned area detection is presented in Fig. 2. First, we applied the BFAST Monitor algorithm for segmentation of stable periods without land cover change by using NDVI time series. Next, a harmonic model was fitted using BAI for each stable

period. By comparing model predictions with the observed values, the outliers caused by fire events were detected. Then, we combined the burned area pixels from each single image into an annual Landsat burned area during fire season. Finally, we made accuracy assessment using reference data interpreted from Landsat images and compared results with MODIS burned area product.

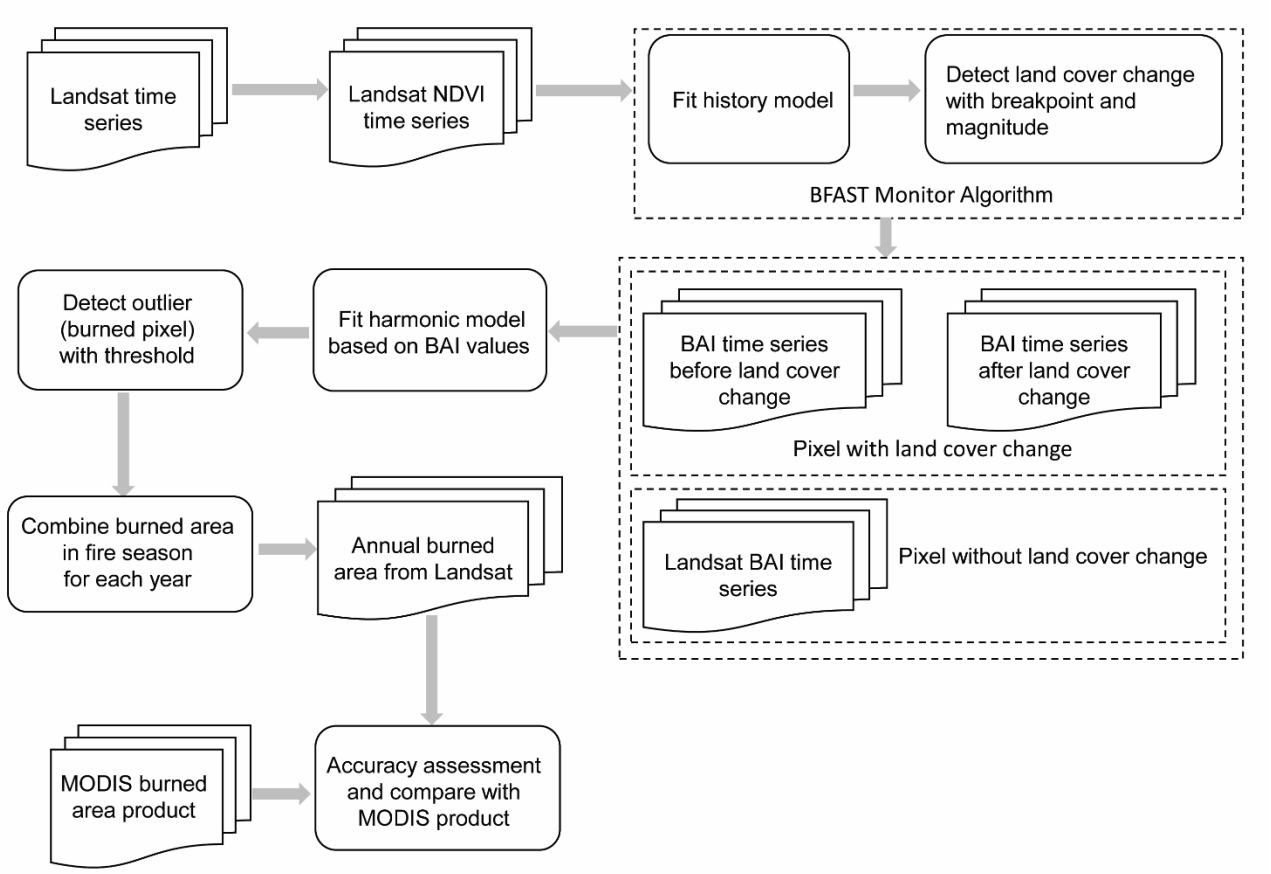

Fig. 2. The main steps of the burned area detection algorithm.

2.3.1 Breakpoint detection in Landsat time series

Land cover change associated with deforestation was detected using the BFAST Monitor (Breaks For Additive Season and Trend Monitor) approach (DeVries et al., 2015). The method fits a harmonic model to NDVI time series in a baseline period, and then compares predictions and observations in the monitoring period. There is little and no observed decline in reflectance in visible and near infrared bands after a savanna fire (Goodwin and Collett, 2014), and burned vegetation recovers quickly, so NDVI time series was used.

Considering that NDVI phenology in the study area follows a first order harmonic model, we fit it (Eq.1) based on observations in a defined baseline period:

$$y_t = a + b \times \sin(\frac{2\pi t}{T} + c) + e_t \quad (1)$$

where y_t is dependent variable (vegetation index), t is independent variable (time as Julian date), T is temporal frequency, a, b and c are model parameters representing the intercept, amplitude and phase component in the harmonic model, respectively, and e_t is the residual error.

The baseline period should be stable and have enough observations for model fitting. We defined the baseline period between October 2000 and October 2002 with a minimum of nine observations for each pixel based on our analysis of the dataset. We fitted the harmonic model for Landsat NDVI time series using ordinary least squares (OLS) linear regression. The model can be applied to make predictions in the monitoring period. By checking the discrepancy between predictions and observations in the monitoring period with a moving sums of residuals (MOSUM) approach, the breakpoint was detected when significant deviation appeared. In addition to breakpoints, the BFAST Monitor algorithm also computed the change magnitude for each pixel by taking the median of all the residuals from observations and predictions in the monitoring period. As the breakpoint may falsely detect land cover change, it cannot be the only criterion for land cover change detection, and the change magnitude layer enables more accurate detection. Given that breakpoints related to positive change magnitudes were not linked to forest disturbance, we only regarded breakpoint pixel with negative magnitude (a threshold of zero) as potential disturbance pixel (DeVries et al., 2015). After detecting land cover change in the NDVI time series, each pixel had its own stable period. The pixel that had disturbance was separated into before and after land cover change periods respectively, and the pixel without land cover change was considered stable for the period from 2000 to 2016.

2.3.2 Burned area detection using BAI time series

In our study area, seasonal fires rarely lead to land cover conversion (Silva et al., 2005). However, they affect the spectral reflectance and indices during the fire season. The burned area detection method utilize the time series model and BAI ($BAI = 1/((0.1-Red)^2+(0.06-NIR)^2)$). The BAI is selected in our study because it is effective for burned area detection in previous studies in savanna area in Africa (Dempewolf et al., 2007). The method consisted of three steps and was applied to Landsat BAI time series data with a stable period. Because some pixels were disturbed and separated into two periods, the method was applied to the time series data before and after land cover change periods, respectively. For the pixels without land cover change, the burned area detection method was applied for the whole period. First, we generated a BAI image stack from Landsat time series. Second, we fitted the time series harmonic model in Equation 1 using all the BAI observations within the stable period as dependent variable. Third, we defined a threshold to detect burned pixels by comparing the observed and predicted BAI values. The threshold was determined by checking its influence for accuracy and was computed as the difference between the predicted value plus the

threshold value multiplied by the root mean square error (RMSE) and the observed value. If the threshold was less than zero, we identified the pixel as a burned pixel and removed it from the time series. Otherwise, if the threshold was greater than or equal to zero, the pixel was regarded as an unburned pixel. In cases where not all burned pixels could be detected in a single step, we applied the method iteratively. The harmonic model was fitted using an iteratively-reweighted least squares method, which is robust against outliers (Zhu and Woodcock, 2014a). This meant that we repeated the process until no more outliers were detected.

2.3.3 Annual burned area from Landsat

To obtain annual burned area, we combined the burned area detection results from separate images during the fire season. The fire season was defined as lasting from the early fire season to the late fire season in next year. However, the early and late fire seasons varied from year to year in our study area. In order to make the comparisons of burned area from Landsat and MODIS consistent in time, the precise fire season was determined by checking the date from MODIS burned area product. The pixels were classified into burned and unburned types. The definition of the fire season reduced errors in the burned area detection, because we could eliminate false detections caused by cloud shadows and cropland in other months.

2.4 Accuracy assessment and comparison with MODIS products

It is difficult to obtain reference data for burned area detection over a long time period. Therefore, we obtained reference data for accuracy assessment by visual interpretation of the Landsat time series, which is a practical method indicated in previous studies (Stroppiana et al., 2012; Goodwin and Collett, 2014). We sampled 70 points based on random systematic sampling. The distance between the points was 10 km in west-east direction and 10 km in north-south direction in order to cover the whole study area. Hence, there were 1120 points in total given the 16 years of observations. For each point (pixel) and year, we interpreted whether the pixel was burned in that particular year using all the available observations. Finally, the annual and overall accuracies were calculated by comparing the visually interpreted reference data and Landsat derived burned area for the same pixels.

We derived burned area from MODIS burned area product (MCD45A1) between October 2000 and April 2016. The MODIS burned area product (MCD45A1) provides a monthly gridded 500 m product with the burning time, the spatial distribution of burned area and quality information. The burn scars are detected by a bi-directional reflectance model-based change detection approach in MODIS reflectance time series (Roy et al., 2002; Roy et al., 2005; Roy et al., 2008). We extracted burn scars and processed them to an annual burned area product based on the burning date.

We evaluated the performance of Landsat derived burned area in comparison to MODIS burned area product at regional scale. More specifically, we used a 5×5 km grid to estimate the proportion of burned area from Landsat and MODIS burned area product.

3 Results

3.1 Breakpoint detection by BFAST algorithm

The BFAST Monitor algorithm was capable of identifying deforestation from stable trajectories, although the time series data is irregular. We selected three pixels to demonstrate how the algorithm detected deforestation (Fig. 3). It is expected that events such as deforestation lead to a decrease in NDVI, whereas stable areas should have NDVI values distributed along the predicted model. In Fig. 3a, a breakpoint in 2006 is identified, and the decreased NDVI results in a negative magnitude of -0.148. The time series in Fig. 3b shows a breakpoint in 2004, with a positive magnitude of 0.023. As the disturbance should be determined by the breakpoint and negative magnitude together, we still regarded the time series in Fig. 3b as stable. In Fig. 3c, there is no breakpoint, and the magnitude is positive, indicating it to be a stable time series. By visual interpretation of the time series in Fig. 3c, we observed that a fire took place during December 2013. The fire occurred in the dry season which is a characteristic of fires in our study area. However, it was not detected as a breakpoint in the pixel time series, because the NDVI value for vegetation is also low in dry season, and the difference between NDVI values from burned and unburned pixels is small.

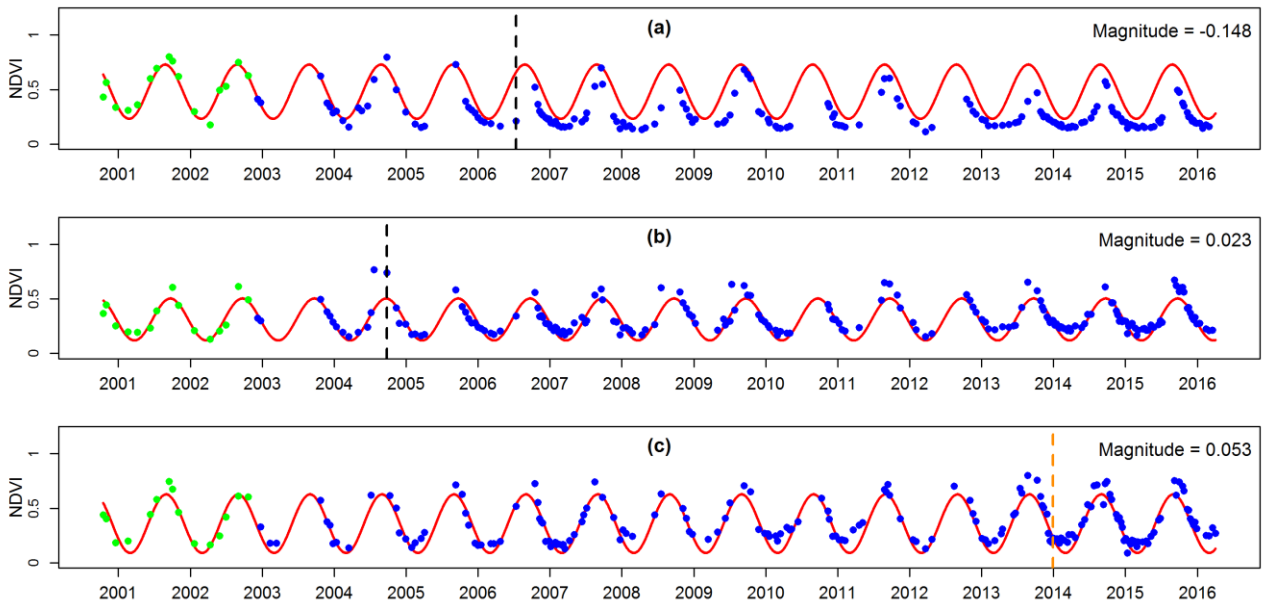

Fig. 3. Demonstration of three pixel-wise time series. The green points are NDVI values in the baseline period, the red curve is the harmonic model fitted in the baseline period and predicted in

monitoring period, the green points are NDVI values in monitoring period, the black vertical line shows the breakpoint and the orange vertical line shows the fire event.

The disturbance map generated using the breakpoint and magnitude is shown in Fig. 4. Conversion from forest and woodlands to cropland was the main cause of land cover change during the monitoring period. Most land cover changes happened in the south-eastern part of the study area.

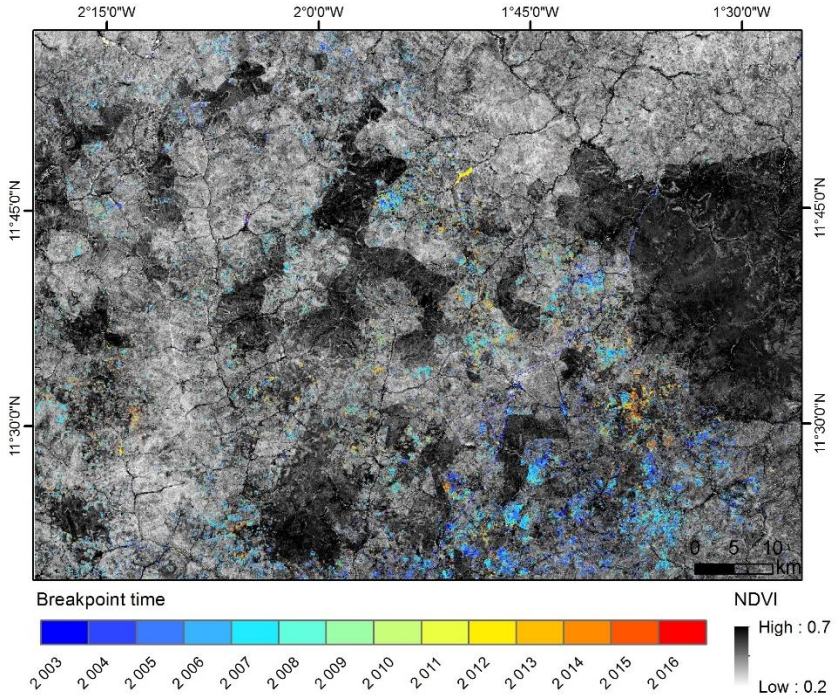

Fig. 4. The detected land cover change on top of NDVI image acquired on 27 October 2013.

3.2 Burned area detection using BAI time series

Fig. 5 demonstrates burned area detection for a stable pixel BAI time series. The burned pixels had higher BAI values compared to unburned pixels, and they appeared as outliers in the harmonic model. The dates of the outliers showed that they occurred during the fire season. We checked the detected outliers with Landsat images, and the results indicated that they were burned pixels. In addition, in most cases, not all burned pixels can be detected at once, and the algorithm should be applied iteratively to detect all burned pixels. In this example, all the outliers were removed after ten iterations.

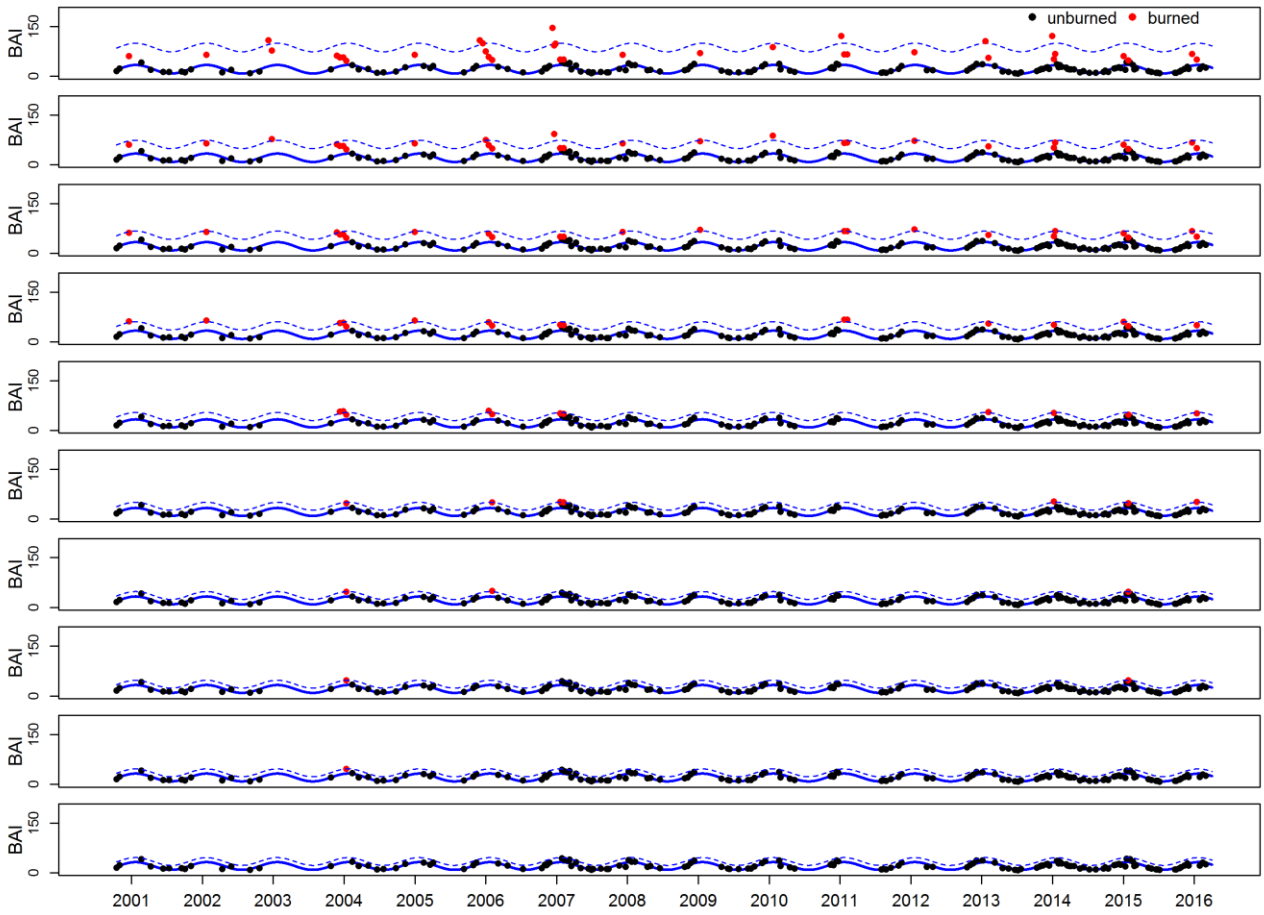

Fig. 5. Demonstration of burned area detection for a single pixel based on burned area index (BAI) time series. The black points are the BAI values, the red points are outliers, the blue curve is the harmonic model, and the dashed blue line is the threshold for detecting outliers. The outliers are considered as possibly burned areas. No breakpoint was detected for this pixel.

Fig. 6 demonstrates the fire detection process for a BAI time series with breakpoint. The algorithm identified a breakpoint in 2013 and divided the time series into two periods. Visual interpretation showed that this particular disturbance was caused by land cover conversion from woodland to cropland. We then fitted harmonic models for the two periods, and all the outliers were removed after eight iterations. During the period before the breakpoint, the outliers detected were all correctly classified as burned, which occurred during the fire season between December and February. Three outliers were detected in the period after the breakpoint. However, these occurred during July and October, which are months outside the fire season. Hence, although they were detected as outliers, they were not regarded as burned pixels. Further visual interpretation confirmed that these pixels represented agricultural land.

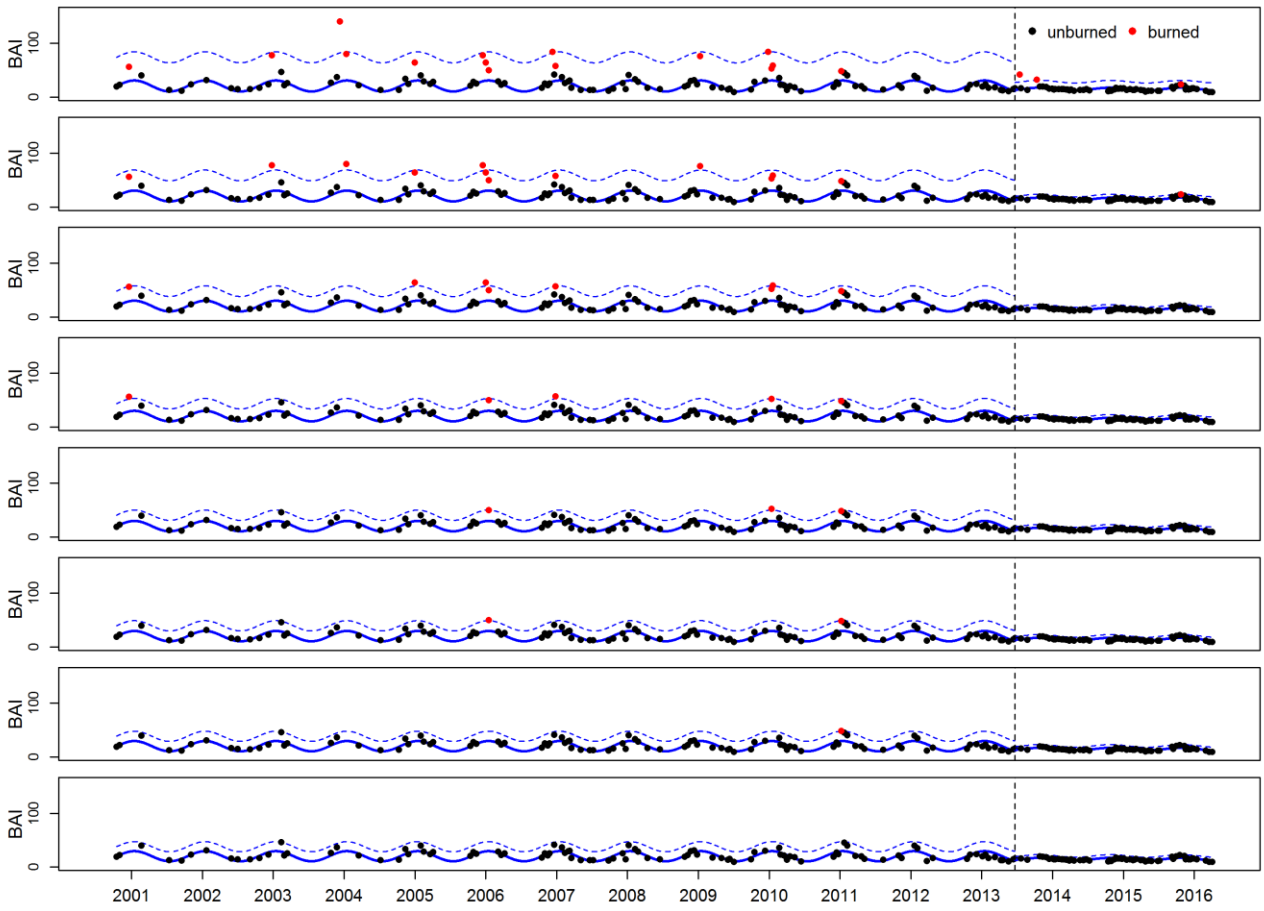

Fig. 6. Demonstration of burned area detection for a BAI time series with breakpoint. The black vertical line shows the breakpoint. The time series is divided into periods before and after the breakpoint. The black points are the BAI values in the time series data, the red points are outliers in the detection approach, the blue curves are the harmonic models for each period, and the dashed blue curves are the thresholds for detecting outliers for each period.

3.3 Accuracy assessment

We evaluated the overall accuracy, producer's accuracy and user's accuracy of burned area detection for a range of thresholds (Fig. 7). With an increasing threshold, the user's accuracy for burned area increased from 60.3% to 89.0%, while in contrast, the producer's accuracy for burned area decreased from 92.3% to 41.1%. The crossing point for the producer's and user's accuracy occurred at a threshold of 2.8 × RMSE. The overall accuracy increased from 67.6% to the peak value of 79.2% at the threshold of 3 × RMSE, and then decreased to 69.7% at the threshold of 4 × RMSE. We selected the threshold 3 × RMSE, because the maximum overall accuracy was achieved with this threshold.

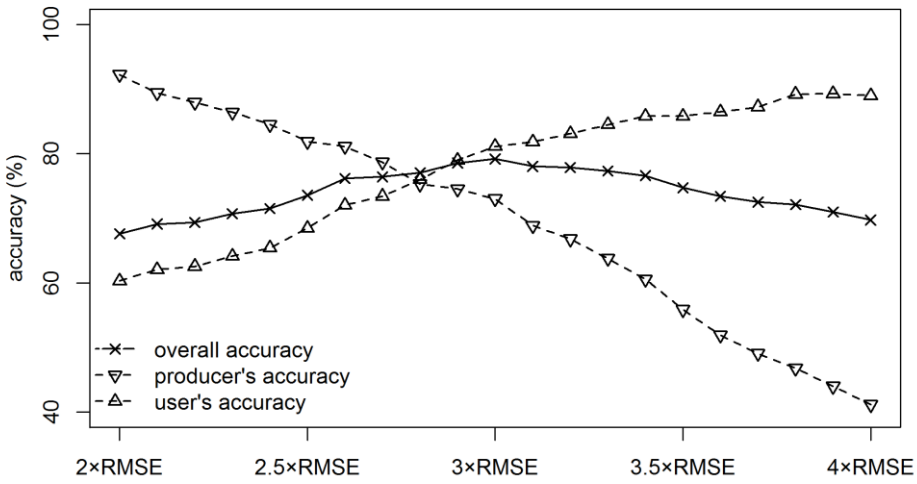

Fig. 7. The dependence of accuracy on the threshold value.

The burned area from Landsat time series achieved a higher overall accuracy (79.2%) than the MODIS burned area product (65.9%) (Fig. 8). The omission error for MODIS burned area product was 62.3%, higher than 26.9% for Landsat burn scars, showing that more burned areas were neglected and detected as unburned in MODIS product. The commission errors for the burned type from Landsat and MODIS burned area product were similar, with values of 18.8% and 20.3%, respectively, revealing that the unburned type was more seldom misclassified as the burned type. The omission error was much higher than the commission error for MODIS burned area product, however, annual burn scars from Landsat had a similar omission error and commission error.

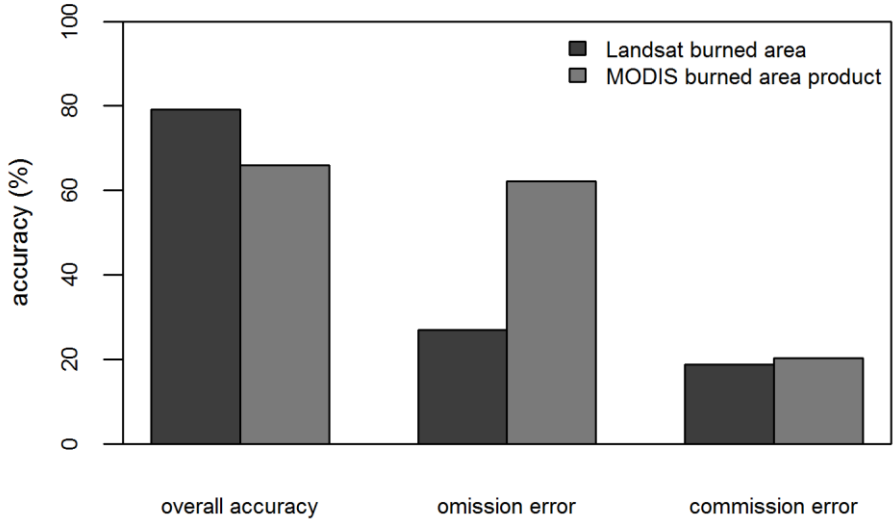

Fig. 8. The overall accuracy, and omission and commission error for the burned type in Landsat and MODIS burned area products.

The overall accuracies of Landsat burned area and MODIS burned area product for each year are shown in Fig. 9. The accuracy of Landsat fire scars was consistently higher than the accuracy of

MODIS burned area product. The overall accuracy of Landsat fire scars ranged from 70.0% to 91.4%. By comparison, the overall accuracy for MODIS burned area product was between 57.1% and 77.1%, and there were some fluctuations over the 16 year period. The accuracies for Landsat burn scars and MODIS burned area product over the 16 year period followed a similar pattern. We observed that the peak values of overall accuracy appeared during 2014–2015 for both Landsat burn scar and MODIS burned area product.

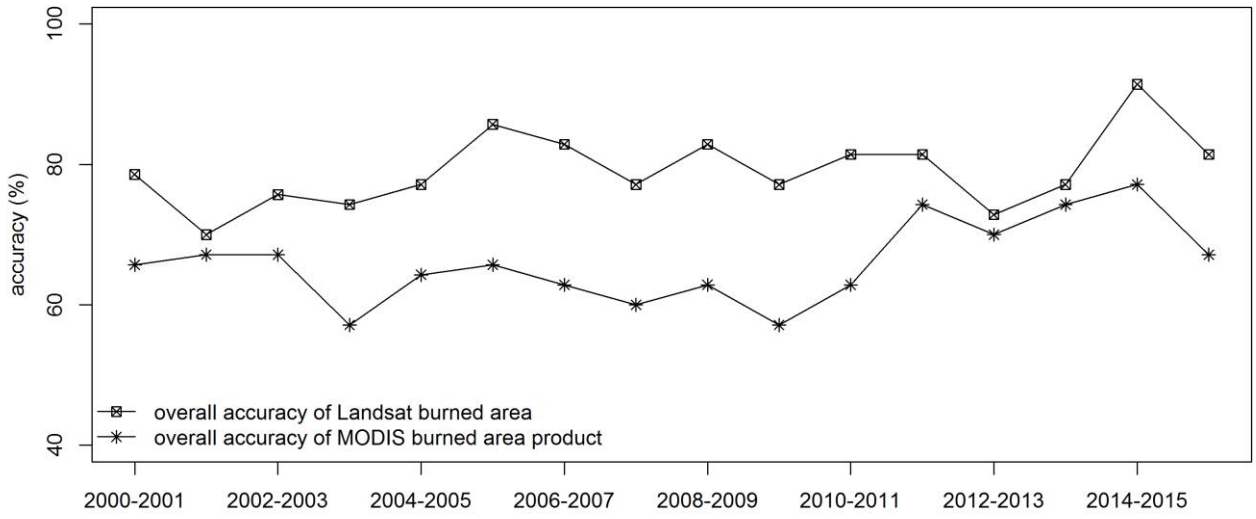

Fig. 9. Annual variation in the overall accuracies of Landsat burned area and MODIS burned area product.

3.4 Comparison with MODIS burned area product

Fig. 10 shows the proportion of burned area in 5×5 km grid cells, with MODIS burned area product (y-axis) and the burned area from Landsat (x-axis). The color scheme illustrates the number of grid cells having the same proportion values. The slope of 0.52 for the burned area from Landsat against MODIS burned area product indicated that the MODIS burned area product underestimated burn scars compared to Landsat burned area. More specifically, we observe that the burned proportion values for Landsat burned area ranging from 0.1 to 0.3 have a higher frequency in Fig. 10, while the corresponding values of the MODIS burned area product are around zero. MODIS burned area product showed poor agreement with burn scars from Landsat with a low R^2 value of 0.30.

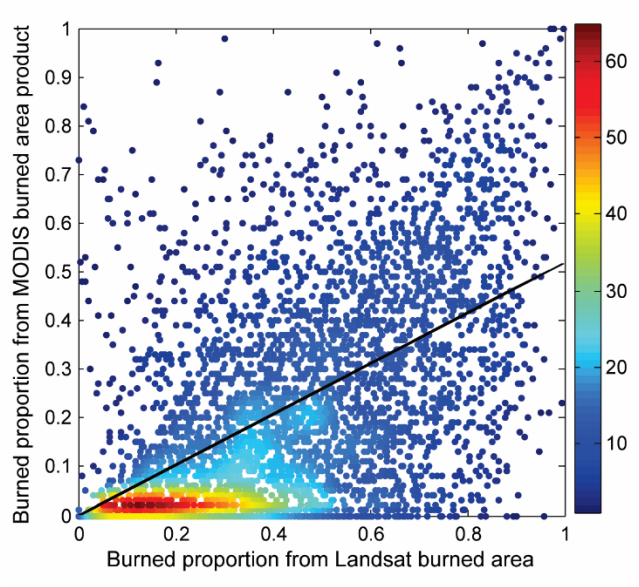

Fig. 10. Comparison of the proportion burned area in 5×5 km grid: Landsat versus MODIS burned area product (slope = 0.52, R^2 = 0.30). The color scheme illustrates the number of grid cells having the same proportion values.

Furthermore, we calculated the burned area percentage for annual Landsat burned area and MODIS burned area product, respectively. The Landsat burned area reported a higher burned percentage than MODIS burned area product, except for 2001-2002, and the comparison indicated that the burned areas were underestimated by MODIS burned area product in comparison to Landsat burned area.

Table 1. Percentage of the study area burned annually based on Landsat burned area and MODIS burned area product.

Burned Percentage	2000-2001	2001-2002	2002-2003	2003-2004	2004-2005	2005-2006	2006-2007	2007-2008	2008-2009	2009-2010	2010-2011	2011-2012	2012-2013	2013-2014	2014-2015	2015-2016
Landsat burned area	0.54	0.27	0.43	0.76	0.51	0.61	0.55	0.27	0.39	0.49	0.66	0.23	0.39	0.29	0.26	0.24
MODIS burned area product	0.44	0.39	0.34	0.37	0.27	0.40	0.22	0.13	0.17	0.17	0.17	0.16	0.06	0.09	0.09	0.09

A spatial comparison of the Landsat burn scar and MODIS burned area product for 2010-2011 and 2011-2012 are shown in Fig. 11. These two periods were selected because the differences of burned percentage from Landsat and MODIS product were largest and smallest for 2010-2011 and 2011-2012, respectively. Landsat burned area and MODIS burned area product had a consistency in burned area distribution in large areas, but Landsat imagery was capable of detecting smaller patches of burned area. However, the Landsat burned area misclassified cropland as burned.

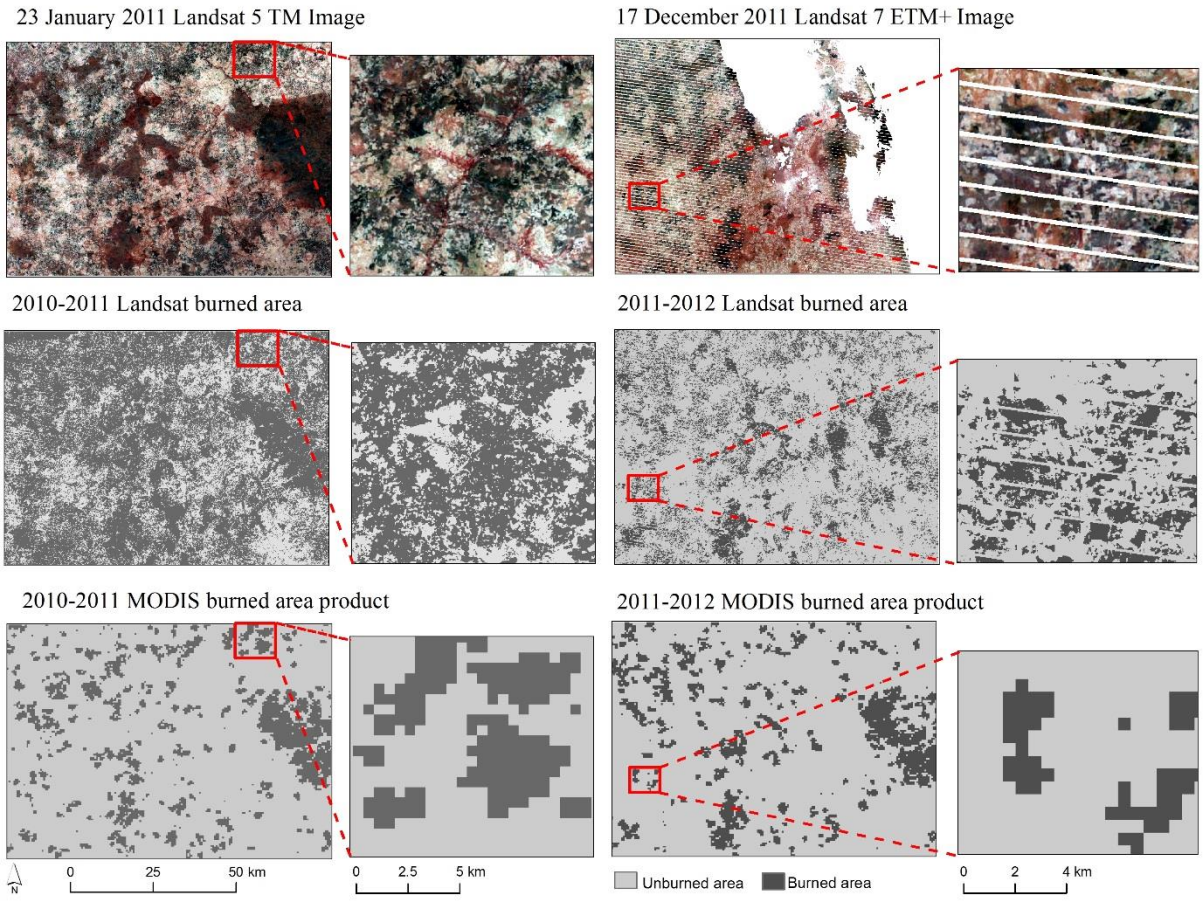

Fig. 11. Comparison of annual Landsat burned area and MODIS burned area for 2010-2011 and 2011-2012. Landsat 5 TM image (RGB: NIR, red and green bands; image acquired: 23 January 2011) and Landsat 7 ETM+ image (RGB: NIR, red and green bands; image acquired: 17 December 2011) are shown as fire season images.

4 Discussion

From our results, we observed that both Landsat burned area and MODIS burned area product were able to capture relatively large and continuous burn scars. However, the burn scars in West African savannas are gradual and heterogeneous in characteristic (Silva et al., 2005). This fragmented pattern of burned area poses a problem for detection. The results indicated that the two coarse resolution burned area products underestimated the burned area compared to our annual burn scar based on Landsat time series, and this result was in line with earlier studies (Laris 2005; Silva et al., 2005; Roy and Boschetti, 2009). The underestimation can be explained by the difference in spatial resolution, as small and fragmented burn scars are difficult to detect at the resolution of MODIS, which demonstrates the importance of a higher spatial resolution in detection. Roy et al. (2008) pointed that the accuracy of MODIS burned area product varied according to the tree cover, suggesting that fire scars mapping should also consider different tree cover conditions. The accuracy pattern with higher

errors of omission than commission for MODIS burned area product observed in our study was consistent with the results of Roy and Boschetti (2009).

The fire season in our study area normally lasts from November to February. Because of this long fire season, the landscape is a patchwork of burn scars of various severity and vegetation in different stages of recovery. The rapid recovery of vegetation makes the old burn scars less obvious and demonstrates similar spectral characteristics compared to unburned area (Hardtke et al., 2015). Therefore, low severity burn scars are not easily detected by our method, causing omission errors. This error is related to the temporal resolution of the sensor, as imagery is not necessarily captured soon after a fire, when the burn scars are best detected. The influence of the temporal resolution of Landsat imagery on burned area detection accuracy have been reported in previous studies (Koutsias et al., 2013; Boschetti et al., 2015, Goodwin and Collett, 2014). With open access to Landsat 8 OLI data and Sentinel-2 data, the temporal resolution of medium spatial resolution imagery has been improved, resulting in a denser time series (Wulder et al., 2015). Future research should investigate the effect of combing all Landsat data and Sentinel-2 data for burned area detection.

Another source of error arose from the unmasked cloud shadows, which showed large BAI values and can cause false burned area detection. This could partly contribute to the overestimation of burned area from Landsat. Furthermore, in some images, the unburned cropland and forest were spectrally similar to burned areas in terms of BAI, which also complicated the burned area detection in the study area. The errors caused by crop harvesting, rapid vegetation senescence, agricultural areas and dark soils have also been reported in previous studies (Stroppiana et al., 2012; Boschetti et al., 2015). In our study, we combined burn scars from each image within the fire season annually, which helped us to exclude other incorrect detections caused by cloud shadows and cropland in wet season months. It could also be possible to use another spectral index to eliminate mixed pixels and improve detection accuracy in future research (Bastarrika et al., 2011; Schepers et al., 2014). It was also reported in other studies that grassland and woodland were frequently burned, and agricultural fields were only seldom burned in Burkina Faso (Devineau et al., 2010; Gessner et al., 2015). Hence, the burned area detection accuracy could be improved by including land cover type information in the algorithm.

Combining Landsat time series and harmonic model fitting proved to be an effective method for annual burned area detection in the study area. It was also demonstrated by Zhu and Woodcock (2014a) that temporal information and harmonic model could be successfully applied for cloud and shadow screening and land cover change detection based on Landsat time series. In addition, there is no need to select training burned pixels in our algorithm, and the algorithm can automatically provide burned pixels as seeds for further analysis with region growing segmentation method (Bastarrika et

al., 2011). Although the annual burned areas from Landsat imagery are encouraging, one disadvantage of the method is the lack of a precise burning date. This is due to the lower temporal resolution of Landsat imagery in comparison to coarser resolution MODIS data. The error arising from the disturbance detection with the BFAST Monitor algorithm could also lead to failure in constructing an accurate harmonic model for BAI time series, and affect the burned area detection accuracy.

With the BFAST Monitor algorithm, we could detect land cover change associated with deforestation during the 16 year period before burned area detection with harmonic model. This is necessary in the area with rapid and ongoing land cover changes. Although there are gaps in the Landsat time series due to the clouds and missing lines, the BFAST Monitor algorithm proved to be effective in detecting land cover conversions in our study area. Similarly to Gessner et al. (2015), we found that there was an increase in the agricultural area at the expense of forest and woodlands. There were also some limitations in our study. We assumed that there was only one time of land cover conversion for Landsat time series over 16 years when we applied the BFAST Monitor algorithm. This is probably a valid assumption for this study, but less applicable for longer time series and sites with repeated land cover conversions. The shifting cultivation (fallow period) does not cause abrupt land cover change as woody cover increases gradually. Furthermore, if fallow lasts only for a short period, its effect on BAI time series model fitting is small. Furthermore, we defined October 2000 to October 2001 as the baseline period to construct the harmonic model, assuming this to be a stable period. However, it can be difficult to choose a stable period in areas that undergo many land cover conversions, and the requirement for a stable baseline period can constrain the application of the BFAST Monitor algorithm.

5 Conclusions

We explored the potential of using Landsat time series for annual burned area mapping based on harmonic model and breakpoint identification. The algorithm used 281 Landsat imageries between October 2000 and April 2016, and the results were compared with MODIS burned area product. The results demonstrated that our algorithm was able to detect small patchy burn scars with a balance of omission and commission errors. In contrast, the MODIS burned area product had a high rate of omission errors and underestimated the total burned area. Given the diverse characteristics of burned areas and land cover types, as well as the decreased data availability due to clouds and missing lines of ETM+ SLC-off images, the Landsat burned area performed well in the savanna area, and achieved a higher accuracy than products using coarser resolution data. The framework that includes spectral

information from medium spatial resolution time series and breakpoint detection should be applicable to other savanna regions, although the same spectral indices (i.e., BAI) and thresholds may not be suitable in other environments. Finally, our results indicate that higher resolution burned area mapping has a high potential to foster local scale decision making on land management with better accuracy and lower costs for end-users.

Acknowledgments

This work was supported by the Ministry for Foreign Affairs of Finland under Building Biocarbon and Rural Development in West Africa (BIODEV) project and China Scholarship Council.

References

Archibald, S., Roy, D. P., van Wilgen, B.W., Scholes, R.J., 2009. What limits fire? An examination of drivers of burnt area in Southern Africa. Glob. Chang. Biol. 15, 613-630.

Bastarrika, A., Alvarado, M., Artano, K., Martinez, M.P., Mesanza, A., Torre, L., Ramo R., Chuvieco, E., 2014. BAMS: A tool for supervised burned area mapping using Landsat data. Remote Sens. 6, 12360-12380.

Bastarrika, A., Chuvieco, E., Martín, M.P., 2011. Mapping burned areas from Landsat TM/ETM+ data with a two-phase algorithm: Balancing omission and commission errors. Remote Sens. Environ. 115, 1003-1012.

Boschetti, L., Roy, D.P., Justice, C.O., Humber, M.L., 2015. MODIS–Landsat fusion for large area 30m burned area mapping. Remote Sens. Environ. 161, 27-42.

Chuvieco, E., Martin, M.P., Palacios, A., 2002. Assessment of different spectral indices in the red-near-infrared spectral domain for burned land discrimination. Int. J. Remote Sens. 23, 5103-5110.

Coulibaly-Lingani, P., Savadogo, P., Tigabu, M., Oden, P.C., 2011. Factors influencing people's participation in the forest management program in Burkina Faso, West Africa. Forest Policy Econ. 13, 292-302.

Dempewolf, J., Trigg, S., DeFries, R. S., Eby, S., 2007. Burned-area mapping of the Serengeti–Mara region using MODIS reflectance data. IEEE Geosci. Remote Sens. Lett. 4, 312-316.

Devineau, J.L., Fournier, A., Nignan, S., 2010. Savanna fire regimes assessment with MODIS fire data: their relationship to land cover and plant species distribution in western Burkina Faso (West Africa). J. Arid Environ. 74, 1092-1101.

DeVries, B., Verbesselt, J., Kooistra, L., Herold, M., 2015. Robust monitoring of small-scale forest disturbances in a tropical montane forest using Landsat time series. Remote Sens. Environ. 161, 107-121.

Disney, M. I., Lewis, P., Gomez-Dans, J., Roy, D., Wooster, M. J., Lajas, D., 2011. 3D radiative transfer modelling of fire impacts on a two-layer savanna system. Remote Sens. Environ. 115, 1866-1881.

Dwyer, E., Pinnock, S., Grégoire, J.M., Pereira, J.M.C., 2000. Global spatial and temporal distribution of vegetation fire as determined from satellite observations. Int. J. Remote Sens. 21, 1289-1302.

Gessner, U., Knauer, K., Kuenzer, C., Dech, S., 2015. Land surface phenology in a West African savanna: impact of land use, land cover and fire. In: Kuenzer, C., Dech, S., Wagner, W. (Eds.), Remote Sensing Time Series. Springer International Publishing, Dordrecht, pp. 203-223.

Giglio, L., Descloitres, J., Justice, C.O., Kaufman, Y.J., 2003. An enhanced contextual fire detection algorithm for MODIS. Remote Sens. Environ. 87, 273-282.

Giglio, L., Randerson, J. T., van der Werf, G.R., Kasibhatla, P.S., Collatz, G.J., Morton, D.C., DeFries, R.S., 2010. Assessing variability and long-term trends in burned area by merging multiple satellite fire products. Biogeosciences. 7, 1171-1186.

Goodwin, N.R., Collett, L.J., 2014. Development of an automated method for mapping fire history captured in Landsat TM and ETM+ time series across Queensland, Australia. Remote Sens. Environ. 148, 206-221.

Hardtke, L.A., Blanco, P.D., del Valle, H.F., Metternicht, G.I., Sione, W.F., 2015. Semi-automated mapping of burned areas in semi-arid ecosystems using MODIS time-series imagery. Int. J. Appl. Earth Obs. Geoinf. 38, 25-35.

Hijmans, R.J., Cameron, S.E., Parra, J.L., Jones, P.G., Jarvis, A., 2005. Very high resolution interpolated climate surfaces for global land areas. Int. J. Climatol. 25, 1965-1978.

Knauer, K., Gessner, U., Fensholt, R., Forkuor, G., Kuenzer, C., 2017. Monitoring agricultural expansion in Burkina Faso over 14 years with 30 m resolution time series: the role of population growth and implications for the environment. Remote Sens. 9, 132.

Kontoes, C.C., Poilve, H., Florsch, G., Keramitsoglou, I., Paralikidis, S., 2009. A comparative analysis of a fixed thresholding vs. a classification tree approach for operational burn scar detection and mapping. Int. J. Appl. Earth Obs. Geoinf. 11(5), 299-316.

Koutsias, N., Mallinis, G., Karteris, M., 2009. A forward/backward principal component analysis of Landsat-7 ETM+ data to enhance the spectral signal of burnt surfaces. ISPRS J. Photogramm. Remote Sens. 641, 37-46.

Koutsias, N., Pleniou, M., Mallinis, G., Nioti, F., Sifakis, N.I., 2013. A rule-based semi-automatic method to map burned areas: exploring the USGS historical Landsat archives to reconstruct recent fire history. Int. J. Remote Sens. 34, 7049-7068.

Laris, P.S., 2005. Spatiotemporal problems with detecting and mapping mosaic fire regimes with coarse-resolution satellite data in savanna environments. Remote Sens. Environ. 99, 412-424.

Laris, P., Wardell, D.A., 2006. Good, bad or 'necessary evil'? Reinterpreting the colonial burning experiments in the savanna landscapes of West Africa. Geogr. J. 172, 271-290.

Liu, J., Heiskanen, J., Aynekulu, E., Maeda, E. E., Pellikka, P.K.E., 2016. Land cover characterization in West Sudanian Savannas using seasonal features from annual Landsat time series. Remote Sens. 8, 365.

Maeda, E.E., Arcoverde, G.F., Pellikka, P. K., Shimabukuro, Y.E., 2011. Fire risk assessment in the Brazilian Amazon using MODIS imagery and change vector analysis. Appl. Geogr. 31, 76-84.

Maeda, E.E., Formaggio, A.R., Shimabukuro, Y.E., Arcoverde, G.F.B., Hansen, M.C., 2009. Predicting forest fire in the Brazilian Amazon using MODIS imagery and artificial neural networks. Int. J. Appl. Earth Obs. Geoinf. 11, 265-272.

Mouillot, F., Schultz, M.G., Yue, C., Cadule, P., Tansey, K., Ciais, P., Chuvieco, E., 2014. Ten years of global burned area products from spaceborne remote sensing-A review: Analysis of user needs and recommendations for future developments. Int. J. Appl. Earth Obs. Geoinf. 26, 64-79.

Musyimi, Z., Said, M.Y., Zida, D., Rosenstock, T.S., Udelhoven, T., Savadogo, P., Leeuw, J.d., Aynekulu, E., 2017. Evaluating fire severity in Sudanian ecosystems of Burkina Faso using Landsat 8 satellite images. J. Arid Environ. 139, 95-109.

Nielsen, T.T., Rasmussen, K., 1997. The distribution in time and space of savanna fires in Burkina Faso as determined from NOAA AVHRR data. Dan. J. Geogr. 97, 86-97.

Olson, D.M., Dinerstein, E., Wikramanayake, E.D., Burgess, N.D., Powell, G.V., Underwood, E.C., D'Amico, J. A., Itoua, I., Strand H.E., Morrison, J.C., Loucks, C.J., Allnutt, T.F., Ricketts, T.H., Kura, Y., Lamoreux, J.F., Wettengel, W.W., Hedao, P., Kassem, K.R., 2001. Terrestrial ecoregions of the world: A new map of life on earth. BioScience. 51, 933-938.

Ouedraogo, I., Savadogo, P., Tigabu, M., Cole, R., Odén, P.C., Ouadba, J.M., 2009. Is rural migration a threat to environmental sustainability in Southern Burkina Faso? Land Degrad. Dev. 20, 217-230.

Ouedraogo, I., Savadogo, P., Tigabu, M., Cole, R., Oden, P.C., Ouadba, J.M., 2011. Trajectory analysis of forest cover change in the tropical dry forest of Burkina Faso, West Africa. Landsc. Res. 36, 303-320.

Plummer, S., Arino, O., Simon, M., Steffen, W., 2006. Establishing a earth observation product service for the terrestrial carbon community: the GlobCarbon initiative. Mitig. Adapt. Strategies Glob. Chang. 11, 97-111.

Roy, D.P., Boschetti, L., 2009. Southern Africa validation of the MODIS, L3JRC, and GlobCarbon burned area products. IEEE Trans. Geosci. Remote Sens. 47, 1032-1044.

Roy, D.P., Boschetti, L., Justice, C.O., Ju, J., 2008. The collection 5 MODIS burned area product-Global evaluation by comparison with the MODIS active fire product. Remote Sens. Environ. 112, 3690-3707.

Roy, D.P., Jin, Y., Lewis, P.E., Justice, C.O., 2005. Prototyping a global algorithm for systematic fire-affected area mapping using MODIS time series data. Remote Sens. Environ. 97, 137-162.

Roy, D.P., Lewis, P.E., Justice, C.O., 2002. Burned area mapping using multi-temporal moderate spatial resolution data-A bi-directional reflectance model-based expectation approach. Remote Sens. Environ. 83, 263-286.

Sawadogo, L., Nygård, R., Pallo, F., 2002. Effects of livestock and prescribed fire on coppice growth after selective cutting of Sudanian savannah in Burkina Faso. Ann. For. Sci. 59, 185-195.

Sawadogo, L., Tiveau, D., Nygård, R., 2005. Influence of selective tree cutting, livestock and prescribed fire on herbaceous biomass in the savannah woodlands of Burkina Faso, West Africa. Agri. Ecosyst. Environ. 1051, 335-345.

Schepers, L., Haest, B., Veraverbeke, S., Spanhove, T., Vanden Borre, J., Goossens, R., 2014. Burned area detection and burn severity assessment of a heathland fire in Belgium using airborne imaging spectroscopy (APEX). Remote Sens. 6, 1803-1826.

Siljander, M., 2009. Predictive fire occurrence modelling to improve burned area estimation at a regional scale: a case study in East Caprivi, Namibia. Int. J. Appl. Earth Obs. Geoinf. 11, 380-393.

Silva, J.M., Sá, A.C., Pereira, J.M. 2005. Comparison of burned area estimates derived from SPOT-VEGETATION and Landsat ETM+ data in Africa: Influence of spatial pattern and vegetation type. Remote Sens. Environ. 96, 188-201.

Smith, A.M.S., Drake, N.A., Wooster, M.J., Hudak, A.T., Holden, Z.A., Gibbons, C.J., 2007. Production of Landsat ETM+ reference imagery of burned areas within Southern African savannahs: comparison of methods and application to MODIS. Int. J. Remote Sens. 28, 2753-2775.

Stroppiana, D., Bordogna, G., Carrara, P., Boschetti, M., Boschetti, L., Brivio, P.A., 2012. A method for extracting burned areas from Landsat TM/ETM+ images by soft aggregation of multiple Spectral Indices and a region growing algorithm. ISPRS J. Photogramm. Remote Sens. 69, 88-102.

Tansey, K., Grégoire, J.M., Defourny, P., Leigh, R., Pekel, J.F., Van Bogaert, E., Bartholomé, E., 2008. A new, global, multi-annual (2000–2007) burnt area product at 1 km resolution. Geophys. Res. Lett. 35.

Verbesselt, J., Zeileis, A., Herold, M., 2012. Near real-time disturbance detection using satellite image time series. Remote Sens. Environ. 123, 98-108.

Wulder, M.A., Hilker, T., White, J.C., Coops, N.C., Masek, J.G., Pflugmacher, D., Crevier, Y., 2015. Virtual constellations for global terrestrial monitoring. Remote Sens. Environ. 170, 62-76.

Zhu, Z., Woodcock, C.E., 2012. Object-based cloud and cloud shadow detection in Landsat imagery. Remote Sens. Environ. 118, 83-94.

Zhu, Z., Woodcock, C.E., 2014a. Continuous change detection and classification of land cover using all available Landsat data. Remote Sens. Environ. 144, 152-171.

Zhu, Z., Woodcock, C.E., 2014b. Automated cloud, cloud shadow, and snow detection in multitemporal Landsat data: An algorithm designed specifically for monitoring land cover change. Remote Sens. Environ. 152, 217-234.